PNAS RESEARCH ARTICLE | ECOLOGY
EARTH, ATMOSPHERIC, AND PLANETARY SCIENCES

Microbially induced precipitation of silica by anaerobic methane-oxidizing consortia and implications for microbial fossil preservation

Daniela Osorio-Rodriguez[a,1,2], Kyle S. Metcalfe[a,1], Shawn E. McGlynn[a,b], Hang Yu[a,c], Anne E. Dekas[a,d], Mark Ellisman[e], Tom Deerinck[e], Ludmilla Aristilde[f], John P. Grotzinger[a], and Victoria J. Orphan[a,2]

Edited by Donald Canfield, Syddansk Universitet, Odense M., Denmark; received February 7, 2023; accepted November 6, 2023

Authigenic carbonate minerals can preserve biosignatures of microbial anaerobic oxidation of methane (AOM) in the rock record. It is not currently known whether the microorganisms that mediate sulfate-coupled AOM—often occurring as multicelled consortia of anaerobic methanotrophic archaea (ANME) and sulfate-reducing bacteria (SRB)—are preserved as microfossils. Electron microscopy of ANME-SRB consortia in methane seep sediments has shown that these microorganisms can be associated with silicate minerals such as clays [Chen *et al.*, *Sci. Rep.* **4, 1–9 (2014)], but the biogenicity of these phases, their geochemical composition, and their potential preservation in the rock record is poorly constrained. Long-term laboratory AOM enrichment cultures in sediment-free artificial seawater [Yu *et al.*, *Appl. Environ. Microbiol.* **88**, e02109-21 (2022)] resulted in precipitation of amorphous silicate particles (~200 nm) within clusters of exopolymer-rich AOM consortia from media undersaturated with respect to silica, suggestive of a microbially mediated process. The use of techniques like correlative fluorescence in situ hybridization (FISH), scanning electron microscopy with energy dispersive X-ray spectroscopy (SEM-EDS), and nanoscale secondary ion mass spectrometry (nanoSIMS) on AOM consortia from methane seep authigenic carbonates and sediments further revealed that they are enveloped in a silica-rich phase similar to the mineral phase on ANME-SRB consortia in enrichment cultures. Like in cyanobacteria [Moore *et al.*, *Geology* **48**, 862–866 (2020)], the Si-rich phases on ANME-SRB consortia identified here may enhance their preservation as microfossils. The morphology of these silica-rich precipitates, consistent with amorphous-type clay-like spheroids formed within organic assemblages, provides an additional mineralogical signature that may assist in the search for structural remnants of microbial consortia in rocks which formed in methane-rich environments from Earth and other planetary bodies.**

ANME-SRB | methane seeps | microbial biomineralization | amorphous silica | microfossils

The anaerobic oxidation of methane (AOM) is a microbially driven syntrophic process in ocean sediments worldwide that modulates methane flux and mediates the production of authigenic minerals, including carbonates and iron sulfides. AOM is frequently mediated by multicellular consortia of anaerobic methanotrophic archaea (ANME) and sulfate-reducing bacteria (SRB) which couple the oxidation of methane to sulfate reduction (1, 2). The production of one mole each of bicarbonate and sulfide increases porewater alkalinity in two total units in zones of AOM activity per mole of oxidized methane, driving the precipitation of carbonate minerals (3, 4) following Eq. **1**:

$$CH_4(g) + SO_4^{2-}(aq) \rightarrow HS^-(aq) + HCO_3^-(aq) + H_2O. \quad [1]$$

Geochemical modeling (5) and isotope signatures (6, 7) in methane seep carbonates imply rapid precipitation rates during early diagenesis, suggesting that the activity of ANME-SRB consortia within these rocks and sediments stimulate carbonate precipitation (8, 9). Therefore, it is surprising that silicates—not carbonates— with compositions and platy morphologies similar to clay minerals have been found in intimate association with environmental ANME-SRB consortia (10, 11) recovered from methane seep sediments. These clay-like phases and Si-rich cements have been proposed to form on consortia through AOM-initiated dissolution of sedimentary Si-bearing minerals (e.g., clays, quartz, or diatom frustules) followed by reaction between dissolver porewater silicon (Si) and metal cations adsorbed to extracellular polymeric substances (EPS) coating ANME-SRB consortia exteriors, and possibly serving as sites for microbial surface adhesion (10). However, as these phases have thus far only been observed on ANME-SRB consortia recovered from methane seep sediments, the extent to which ANME-SRB consortia directly mediated

Significance

Anaerobic methanotrophic archaea (ANME) and sulfate-reducing bacteria (SRB) often associate as multicelled consortia in methane seep sediments and carbonates, with a poorly understood preservation potential in the rock record. Here, we provide evidence for microbially enhanced precipitation of an amorphous silica-rich phase on the exterior of ANME-SRB consortia both in methane-rich sediments, carbonates, and a methane-oxidizing laboratory enrichment culture. This consortia-associated mineral phase may represent a newly discovered microbially enhanced biomineralization mechanism, potentially involved in the preservation of fossilized ANME-SRB consortia in ancient methane seep carbonates. Our results expand on the knowledge of microorganisms and metabolisms facilitating silica mineralization, with important implications for the morphological and structural preservation of microbial fossils in deep time on Earth and other planetary bodies.

The authors declare no competing interest.

This article is a PNAS Direct Submission.

[1]D.O.-R. and K.S.M. contributed equally to this work.

[2]To whom correspondence may be addressed. Email: danieosro@gmail.com or vorphan@caltech.edu.

This article contains supporting information online at https://www.pnas.org/lookup/suppl/doi:10.1073/pnas.2302156120/-/DCSupplemental.

Published December 11, 2023.

the precipitation of these phases, as opposed to a passive attachment from the environment, remains unclear.

Understanding the biogenic vs. abiotic factors contributing to the observed Si-rich phases described from uncultured environmental AOM consortia from complex sediment matrices is a challenge. Authigenic silicate precipitation can occur abiotically in sediments through interactions between porewater Si and clay-type aluminosilicates (12). Additionally, microbially mediated sulfate-coupled methane oxidation increases porewater alkalinity, which can further enhance the dissolution of silicon from quartz, diatom frustules, and other sediment hosted silicate minerals, with silica subsequently redepositing on the exteriors of ANME-SRB consortia (10). Finally, microbial surface ligands can also favor the nucleation of amorphous silica, as previously suggested for ANME-SRB consortia (10), and for microorganisms in hot springs and geothermal systems (13).

In this study, we leverage our sediment-free methane-oxidizing anaerobic enrichment cultures of ANME-2 and SRB (14) and laboratory-maintained authigenic seep carbonates with active endolithic AOM consortia (15) to examine the potential production of these Si-rich phases outside of the sediment environment and under chemically controlled laboratory conditions. ANME-SRB consortia in our enrichment cultures have abundant Si-rich nanoparticulate spheres embedded in EPS, while the exteriors of many carbonate-hosted endolithic AOM consortia were encrusted in Si-rich rims. Notably, the de novo production of these Si-rich phases on ANME-SRB consortia in culture occurred from solutions undersaturated with respect to Si. Therefore, it is suggestive of bona fide precipitation of a Si-rich phase under active sulfate-coupled methane oxidation mediated by ANME-SRB consortia, both in cultures and in a diversity of methane seep habitats, including carbonates (15) and sediments.

As authigenic silicates can entomb and preserve organic carbon (16, 17), the involvement of ANME-SRB consortia in facilitating silicate precipitation may enhance the preservation of methane-associated microbial biomass in fossil seep environments, frequently occurring as ^{13}C depleted carbonate mounds and crusts (18, 19). Previous work by our group and others has demonstrated active methanotrophic ANME-SRB consortia living within the interiors of modern seep carbonates (8, 9, 20), and has documented mineral precipitates with consortium-like size and morphology (21). However, we have not yet identified living or fossil ANME-SRB consortia directly in seep carbonates with high preservation potential such as that observed in other microbial ecosystems conferred by early silica precipitation (22). We posit that the silica encrustation of endolithic ANME-SRB consortia within seep carbonates could enhance their long-term preservation and represents a key trait for identifying fossilized ANME-SRB consortia in the rock record.

Results

ANME-SRB Consortia in Sediment-free Enrichment Cultures are Associated with Nanoscale Amorphous Si-rich Spherical Particles. We investigated the hypothesis of ANME and SRB-mediated silicate precipitation (10) by examining anaerobic methane-oxidizing ANME-2 and SRB consortia enriched from seep sediments after 5 y of anoxic cultivation in the laboratory. The inoculum for these slow-growing sediment-free cultures was sourced from a seep sediment, and maintained under methane headspace in artificial seawater as described in ref. 14. Using correlated fluorescence in situ hybridization (FISH), scanning electron microscopy (SEM), and energy dispersive X-ray spectroscopy (EDS) imaging (Fig. 1 *A*–*C*) on the AOM enrichment cultures, we identified multiple AOM consortia in an EPS matrix that were covered with clusters of ~200 nm diameter spherical Si-rich particles (Fig. 1*D*). These were morphologically similar to previously reported amorphous silica-bearing spherical precipitates associated with cyanobacteria in hot springs (23, 24). The SEM imaging of consortium exteriors revealed the universal presence of Si-rich phases in these cultures, often embedded within carbon-rich EPS material connecting clusters of multiple ANME-SRB consortia (*SI Appendix*, Fig. S1). Transmission electron microscopy (TEM) analysis corroborated these findings, showing these Si phases were intimately integrated within the EPS matrix within which many dozens of AOM consortia were embedded (Fig. 1 *E* and *F*). Image analysis of this TEM data estimated a fairly uniform particle size for these silica spheres (230 ± 62 nm, n = 6,060), notably similar to the texture of authigenic silica precipitated during microbial respiration of iron-bearing clays (25). To compare these with environmentally acquired ANME-SRB consortia from seep sediments, we conducted high-resolution nanoscale secondary ion mass spectrometry (nanoSIMS) analysis of the spatial distribution of ^{28}Si on TEM-sectioned consortia (Fig. 2 *A*–*D*), as well as correlated FISH-SEM-EDS on a AOM consortium after Ga^+ focused ion beam milling [Fig. 2 *E*–*G*; (11). These independent analyses both demonstrated that the spatial distribution of silica-bearing particles associated with sediment-hosted ANME-SRB consortia from sediment was similar to that of the Si-rich precipitate observed on AOM consortia grown in sediment-free enrichment cultures (Fig. 1*E*). Specifically, this silica phase is localized to the exteriors of ANME-SRB consortia and is not present surrounding cells within consortia interiors.

Si-rich Phase on AOM Consortia Is Compositionally Distinct from Silica Minerals in Seep Sediment. Chemical analysis of the amorphous silica-rich phase associated with ANME-SRB consortia from our sediment-free enrichment cultures revealed that this phase had a similar composition to the Si-rich phases analyzed on environmental consortia directly extracted from methane seep sediments (Fig. 3*A*), suggesting that the composition of this Si-rich mineral phase is common to AOM consortia despite the large differences in conditions between the in situ seep environment and sediment-free AOM enrichment cultures. Notably, the composition of this amorphous silica-rich phase attached to AOM consortia was distinct from the siliciclastic methane seep sediment particles from which the original inoculum of ANME-SRB consortia was sourced. Mineral phases attached to AOM consortia recovered from both native seep sediments and within our sediment-free cultures typically had lower Si, Al, and Fe (~5–20 atom % Si, ~0–5% Al, and ~0–3% Fe) than the sediment particles which hosted them (~15–25 atom % Si, ~5–10% Al, and ~3–10% Fe; Fig. 3 and *SI Appendix*, Fig. S2). We note that raw atom % values calculated from EDS data may underrepresent Si, Al, and Fe in consortia given the high local C or O from proximal biomass. Thus, we characterized the composition of consortium-attached silica-rich precipitates by ratios of elements typically found in octahedral sites of clays (Mg, Al, Fe) to Si and found that AOM consortia had Al:Si ratios <0.37 and (Mg + Al + Fe):Si ratios <0.5, which are generally lower than those of the sediment from which they were associated (Fig. 3). To determine whether clay-like phases might precipitate with respect to the activity of ions in our artificial seawater media (Dataset S4), we prepared mineral stability diagrams with the solution composition of our experiments (Fig. 3*B* and *SI Appendix*, Fig. S4). The predominant silicate minerals in equilibrium with this solution were clays (kaolinite and illite), feldspar (albite), and chlorite minerals (chamosite and clinochlore) (26). At our specific pH

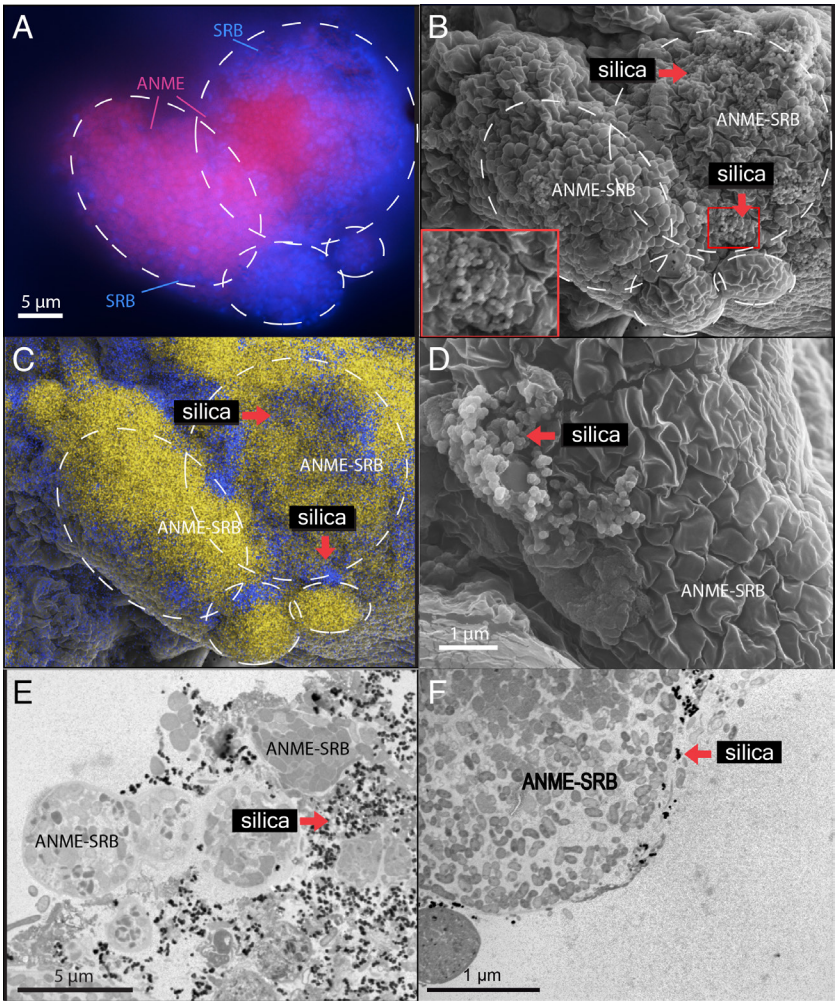

Fig. 1. Epifluorescence and microscopy of sediment-free ANME-2/SRB consortia in laboratory incubations. (*A*–*C*) Correlated FISH, SEM, and EDS imaging of ANME-2/SRB consortia and associated Si-rich phases. Dashed ovals outline individual AOM consortia within the cluster across all three panels. (*A*) FISH image of a cluster of ANME-SRB consortia, with ANME-2 cells stained in pink and inferred SRB cells in blue. (*B*) Paired SEM image of the same cluster of AOM consortia in (*A*) where red arrows denote areas enriched in silica. *Red Inset box*: 2X magnified view of ~200 nm amorphous silica spheres. (*C*) EDS map showing elemental distribution, where yellow is carbon associated with ANME-SRB biomass, with silicon (blue) is concentrated in the extracellular matrix around individual AOM consortia. (*D*) Higher magnification SEM image showing nanoscale silica spheres associated with AOM consortia. (*E* and *F*) TEM cross-section of ANME-SRB consortia and closely associated Si-rich particles (red arrow).

and dissolved Si values, predominantly aluminosilicates related to 1:1 clays were in equilibrium with the solution composition (Fig. 3*B*), suggesting the Si-rich phases associated with ANME-2/SRB consortia may be associated with clays such as kaolinite (Fig. 3*B*). Precipitation of silica (amorphous or crystalline) would require a dissolved Si concentration at three orders of magnitude greater than the concentration in our experiment. Notably, the Si-rich phases attached to ANME-SRB consortia from this work were significantly more enriched in Si than cell-attached silicates previously used as a model for silica precipitation resulting from cation bridging by Fe or Al adsorbed on cell walls (27); (*SI Appendix*, Fig. S3). Furthermore, the Al/Si ratios in the ANME-SRB-associated precipitates were consistently lower than expected in clay compositions (Fig. 3*A*), supporting the biologically mediated process in the Si enrichment in the precipitates.

Precipitated Si-rich Phases Attached to AOM Consortia in Culture. The long-term maintenance of our AOM enrichment cultures and the absence of a sediment matrix provided the opportunity to place additional constraints on the process by which amorphous silicate particles associate with ANME-SRB consortia. We formulated a simple model of ANME-SRB growth, using estimates of ANME-SRB doubling times from the literature (3 to 7.5 mo); (28–32), to roughly determine the maximum number of AOM consortia in the starting inoculum that would have resulted in a larger EPS-embedded aggregation of 55 or more ANME-SRB consortia (e.g., *SI Appendix*, Fig. S5) after 5 y of anaerobic cultivation in sediment-free artificial seawater supplied with methane. Our simplified model assumes that the larger EPS embedded aggregations of AOM consortia observed in culture were formed by consortia growth since these clusters were not observed in the starting inoculum and in early time points of the enrichment. The results of this model (Fig. 3*C*) indicate that a 55-consortium cluster could have grown from no more than 2 consortia, assuming a conservative doubling time of 7.5 mo. Doubling times shorter than ~6 mo in this model imply a 55-consortium cluster would have grown from <1 consortium. Similarly, clusters with less than ~32 consortia with a doubling time of 7.5 mo are calculated to have grown from <1 consortium, suggesting these smaller aggregated AOM clusters formed from consortia during the laboratory incubation that were not originally part of the initial inoculum, or possibly represent clusters that separated from larger aggregations during the incubation or culture processing. Based on the observed and modeled AOM

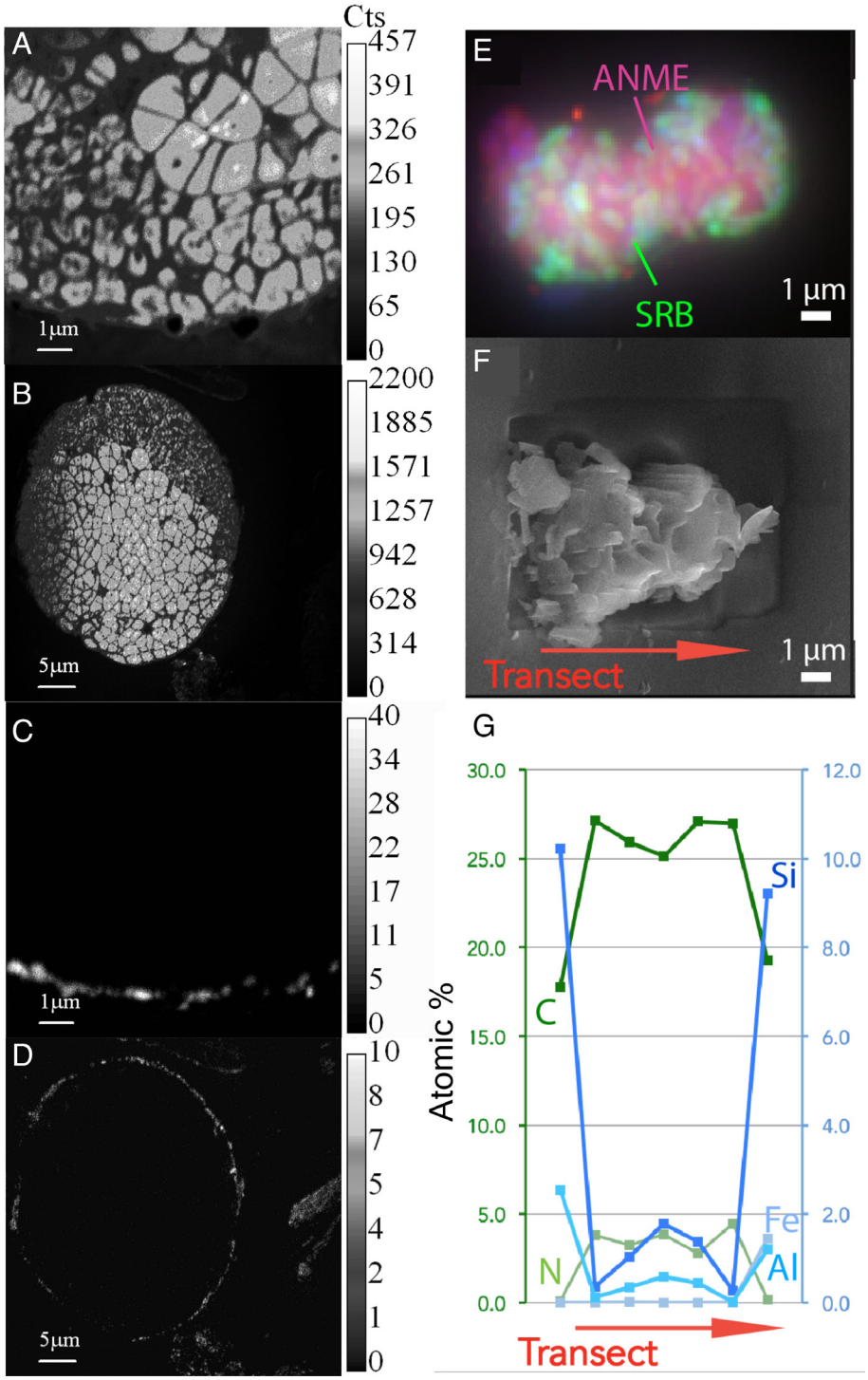

Fig. 2. Images of ANME-SRB consortia isolated from sediments. (*A* and *B*) NanoSIMS $^{12}C^{14}N$ maps; (*C* and *D*) NanoSIMS ^{28}Si maps of the same ANME-SRB consortia shown in (*A* and *B*), respectively, where silicon can be observed forming rims around the consortia. Lighter colors indicate higher counts, shown by the bars to the left of the images. (*E*) FISH of a sediment-associated ANME-SRB consortium, with ANME in pink and SRB in green. (*F*) SEM of the consortium in (*E*) after FIB section. (*G*) Elemental composition by EDS along a transect of the consortium in (*F*), which shows higher C and N relative abundances in the interior and an enrichment in Si and Al at the edges of the consortia.

consortia growth, we reason that the Si-rich phases detected in the extracellular matrix surrounding and in between individual AOM consortia must have developed over the 5-y enrichment period, as essentially all consortia associated with amorphous silica in the enrichment cultures were predicted based on the modeled doubling times to have grown after inoculation.

The concentration of dissolved silica in four sediment-free AOM enrichments and the artificial seawater medium was measured using ICP-MS calibrated standards, and these values were compared with the [Si] equilibria of abiotic processes known to generate amorphous silica, including silica precipitation (33) and sorption of Si to clay minerals (34); (Table 1). Unlike in several previous experiments examining potential microbial silicate biomineralization, where precipitation on bacterial or archaeal cell surfaces was only observed under conditions supersaturated with respect to clay (27, 35, 36) or silica precipitation (37–41), the

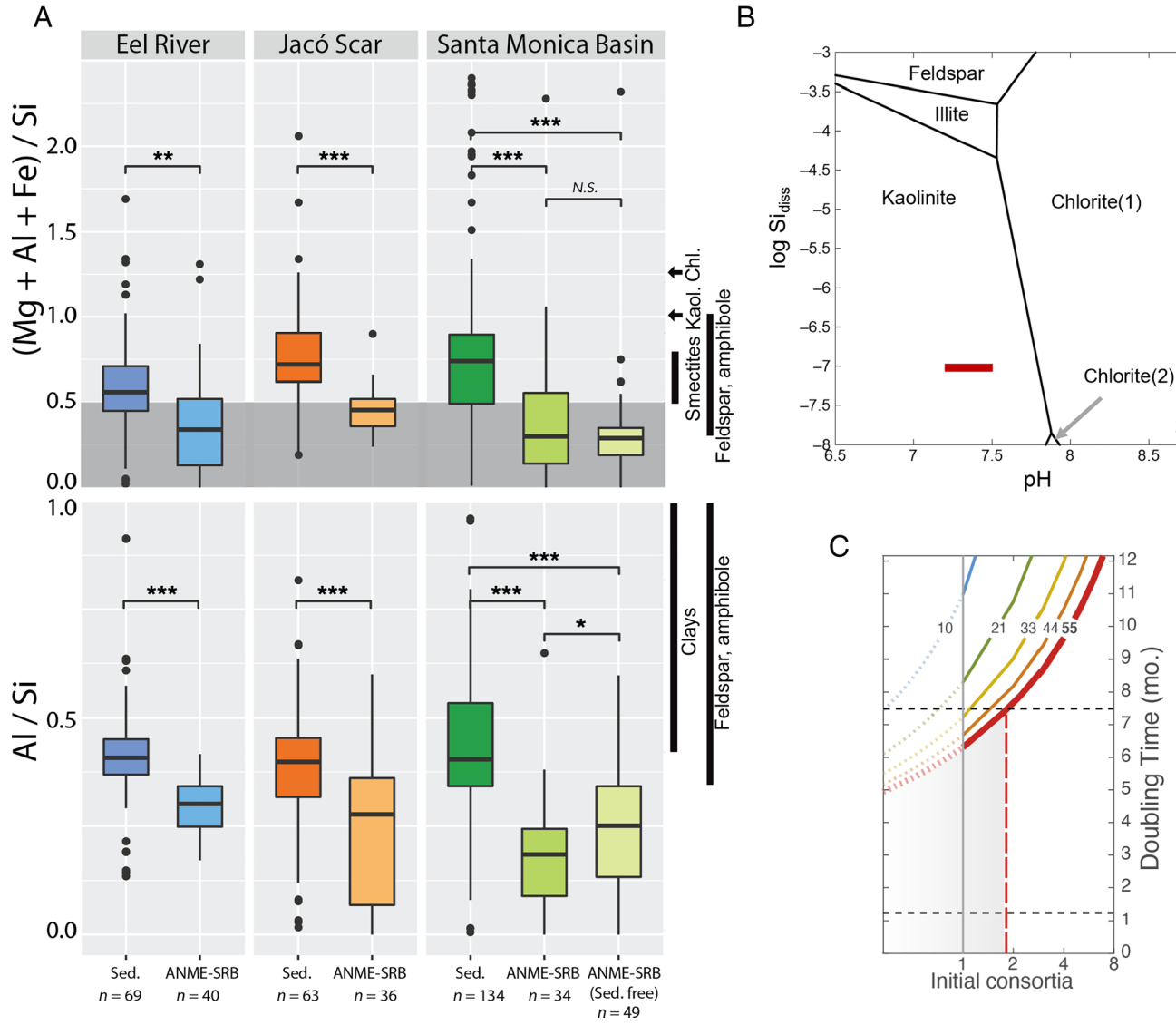

Fig. 3. Composition of Si-rich phases associated with ANME-SRB consortia isolated from sediments and in sediment-free incubations. (*A*) Elemental ratios of EDS-acquired compositional data of ANME-SRB consortium-attached Si-rich phases extracted directly from methane seep sediments ("ANME-SRB") or grown under sediment-free conditions ("sed. free") compared with the range of compositions of sediments from three different seep sediment locations from Northern and Southern California and the Costa Rican margin from which the AOM consortia were recovered ("sed."). Sampling location details can be found in *Materials and Methods*. Reference clay mineral compositions are also noted [arrows on right; montmorillonite (mont), illite (ill), chlorite (chl)]. Also shown is the composition of three different Si-rich rings surrounding carbon-rich cell aggregates in a seep carbonate. (*B*) Predicted mineral stability diagram for silicate mineral formations in the experimental solution composition with both illite, smectite, and kaolinite included as clay minerals. Feldspar refers to albite; Chlorite(1) and Chlorite(2) refer to chamosite and clinochlore, respectively; and the red bar corresponds to ICP-MS measurement of [Si] in artificial seawater media from the sediment-free AOM enrichments. Crystalline or amorphous silica precipitation would require higher dissolved silica and lower pH values. (*C*) A general model of AOM consortia growth showing the estimated final number of consortia (contours) within a cluster as a function of the initial consortia numbers within the enrichment, constrained by the range of reported values for ANME-SRB doubling times (dashed lines).

silica concentrations (21 to 64 μM) in the artificial seawater media and sediment-free enrichments (Table 1) were several orders of magnitude below [Si] for abiotic silicate precipitation [4.3 mM (42). Neither silica or aluminum were directly added to the artificial seawater media (14); however, it is possible that traces of these elements may have leached from the walls of the glass serum vials or were present as part of the original sediments where the aggregates were retrieved from. The active formation of Si-rich phases attached to ANME-SRB consortia in enrichment media undersaturated with respect to Si suggests formation by a yet unknown mechanism that is likely mediated by an aspect of the physiology of the methanotrophic ANME-2 and/or associated SRB partners, given the intimate physical association between silica and AOM consortia in the sediment-free enrichment cultures. It has been shown that monomers of silicic acid can condense forming soluble polymeric silicic acid (PSA) particles which can aggregate at pH <7 (43). Local low pH conditions within ANME-SRB consortia, favorable for PSA formation, may be enhanced by direct extracellular electron transfer between ANME archaea and their SRB partner, where a build-up of protons from methane oxidation is predicted to accumulate resulting in local pH gradients (44), with contributions from silica dissolution and carbonate precipitation (10). Organic polymers may also enhance the condensation of monomeric silicic acid, leading to the formation of silica nanoparticles (43). The specific mechanism of formation and whether organic ligands are responsible for the precipitation of silica on the surfaces of ANME-SRB consortia remains an outstanding question at this time, but with

Table 1. Silica concentrations in sediment-free ANME-SRB incubations and sample locations

Location	Si (μM)	Reference
Santa Monica Basin porewater	110–300	(45)
Costa Rica cold seeps porewater	110–500	(46)
Eel River Basin porewater	700–1000	(47)
ANME-SRB sed-free enrichment 1	63.24	This study
ANME-SRB sed-free enrichment 2	21.08	This study
ANME-SRB sed-free enrichment 3	29.96	This study

continued progress in cultivation for these slow-growing methanotrophic consortia, complementary detailed analyses will likely be possible in the future.

Amorphous Si-rich Minerals Occur on Endolithic ANME-SRB Consortia in Seep Carbonates. The preservation of AOM signatures in paleo-methane seeps primarily exists within authigenic carbonates, where mineral, isotopic, and lipid biosignatures provide evidence for past sulfate-coupled methane oxidation activity catalyzed by ANME and SRB that are analogous to those observed in modern methane seep ecosystems worldwide (21, 48, 49). As the greatest potential for Si-enhanced preservation of microfossils of AOM consortia is likely to be found within authigenic carbonates, we extended our investigation to active endolithic AOM consortia within modern methane seep carbonates and the possibility that these assemblages, like those in sediments and enrichment culture, also showed evidence of silica precipitation. To investigate this possibility, we examined an authigenic carbonate sample composed primarily of calcite collected from an active deep-sea methane seep site found off the coast of Costa Rica (~1,800 m depth). Preliminary analyses of 16S rRNA gene sequences from subsamples of this seep carbonate in our group showed a dominance of ANME-2c and ANME-3 archaea, as well as members of SeepSRB1 active sulfate-coupled AOM activity. Correlated epifluorescence microscopy using the general DNA stain DAPI (Fig. 4*A*) and SEM imaging (Fig. 4*B*) of a resin-embedded and sectioned sample of this seep carbonate revealed ~10–20 μm diameter consortia composed of tightly packed cocci cells. SEM-EDS analysis revealed these electron-dense regions were more C-rich than the surrounding carbonate matrix (Fig. 4*C*) and notably, were directly associated with Si-rich rims (Fig. 4*D*), similar to the environmental ANME-SRB consortia analyzed from seep sediment. FISH hybridization of these embedded endolithic aggregates in thin section confirmed that they were in fact ANME-2/SRB (Fig. 5 and *SI Appendix*, Fig. S6), and correlated SEM (*SI Appendix*, Fig. S7) and EDS of these taxonomically defined consortia (Fig. 5) confirmed the close association of Si with the consortia exteriors (50). FISH hybridization of ANME-SRB aggregates in a carbonate matrix was only recently reported (20), and our work advances the study of endolithic AOM consortia in rock thin sections directly correlated with elemental composition of these consortia and their adjacent matrix. The morphology of the ANME-2/SRB aggregates in the carbonates is consistent with FISH-identified ANME-2/SRB consortia previously observed in sediments identified by FISH (51). Compositional spectra from EDS (Dataset S1) documented low Al, Fe, and Mg content (<0.6 % wt) in Si-rich rings, with (Mg + Al + Fe):Si and Al:Si ratios similar to those of Si-rich phases attached to ANME-SRB consortia recovered directly from seep sediments and in our sediment-free laboratory enrichment cultures (Fig. 3*A*; Datasets S2 and S3). Given the compositional and textural similarities between these Si-rich rings and the Si-rich phases associated with ANME-SRB consortia, we interpreted these Si-rich rings surrounding endolithic aggregates in seep carbonates to be analogous to those found encrusting ANME-SRB consortia originating from sediments.

Discussion

We observed and identified Si-rich phases on ANME-SRB consortium exteriors from seep sediments, authigenic carbonates, and sediment-free AOM enrichment cultures that were incubated in artificial seawater media undersaturated with respect to silica. Measurement of [Si] in sediment-free incubation media via ICP-MS precluded abiotic mechanisms of Si enrichment of consortium-attached Si-rich phases, as [Si] was too low to drive either amorphous silica precipitation or Si sorption on preexisting consortium-attached silicates. Additionally, most consortium-attached phases are enriched in Si with respect to detrital silicates in the sediments from which they were sourced, and also compared to known clay mineral compositions, suggesting that these phases are not simply a product of the attachment of clay minerals in sediment. For example, in Si-rich endmember clay compositions such as montmorillonite $[(Na,Ca)_{0.33}(Al,Mg)_2(Si_4O_{10})(OH)_2{\cdot}nH_2O)]$, with a 2:1 ratio of tetrahedral to octahedral sheets and where Si occupies all tetrahedral sites, the octahedral cation to Si ratio is 0.5 (53); however, consortium-attached Si-rich phases had octahedral cation: Si ratios generally <0.5 (Fig. 3*A*). For comparison, methane seep sediment samples from which consortia were extracted had octahedral cation to Si ratios typically >0.5, consistent with clay minerals (Fig. 3*A*). These results contrast with a previous report of incrustation of AOM consortia with clay minerals (10), however, the phases reported in that study also had cation: Si ratios generally <0.5, implying there also existed minerals more enriched in Si compared to known clay minerals. Our mineral stability diagrams (Fig. 3*B* and *SI Appendix*, Fig. S4) showed that the media solution chemistry was undersaturated with respect to quartz (amorphous or crystalline), but not with respect to clay precipitates, notably kaolinite (Fig. 3*B*). Furthermore, the morphology of our Si-enriched precipitates is not consistent with crystalline clay phases (Fig. 1 and *SI Appendix*, Fig. S1), but rather with the spheroid-like particles expected for the formation of clays within organic assemblages (26). However, the Al/Si content is lower than what is found in clay composition. Altogether, our findings led us to propose that the Si-rich phase associated with AOM consortia was likely a result of two types of biological processes: biomineralization of Si-enriched precipitates from solutions undersaturated with respect to silica and the formation of clay precipitates in intimate associations with the organic/cellular assemblages.

Microbial precipitation of silica in undersaturated conditions has been previously proposed to be mediated by iron (39) and magnesium (54, 55) in solution. Experimental studies in cyanobacteria have shown that sulfate-rich EPS and an increase in pH promoted by photosynthesis enhance the precipitation of magnesium-rich silica, where magnesium likely acts as a cation bridge between positively charged silicic acid and negative functional groups in the EPS (55). Although we did document a carbon-rich rim around two ANME-SRB consortia within the carbonate rock (Figs. 4*B* and 5*A*), consistent with the presence of EPS, this mechanism is not congruent with our observation that the silicates attached to ANME-SRB consortia have low Al, Fe, and Mg content (<0.6 % wt). In this study, Si-rich phases were observed in association with the exteriors of ANME-SRB consortia, consistent with a previously published study (10). This is surprising since cell interiors might be more conducive to silicification in undersaturated conditions, for example, as is observed in the intracellular Si-concentrating mechanisms in diatoms (56), but it is

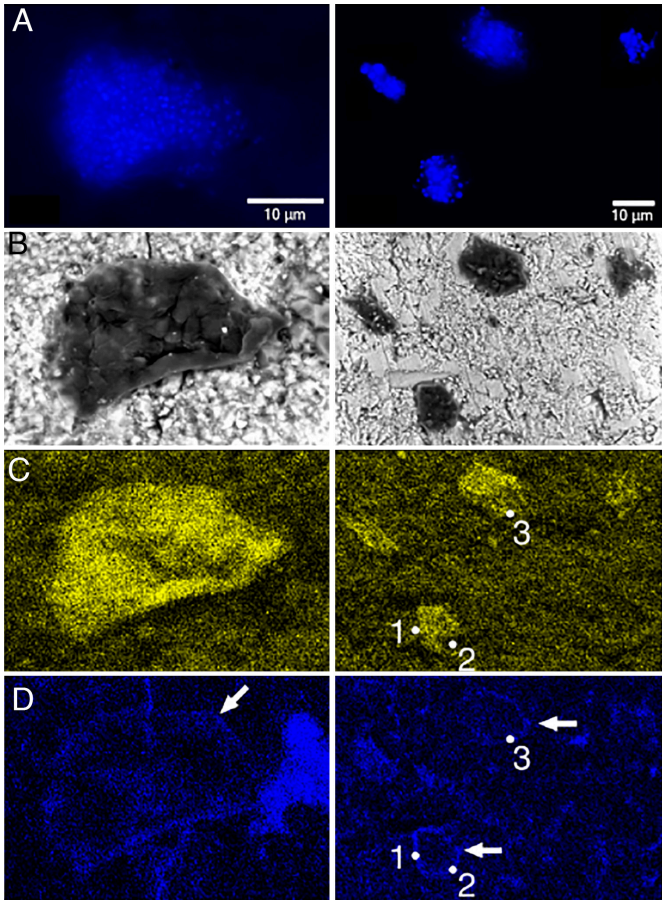

Fig. 4. Correlated epifluorescence microscopy, SEM, and elemental analysis of endolithic microbial consortia and associated Si-rich phases in seep carbonate. (*A*) DAPI-stained putative endolithic ANME-SRB consortia embedded within the seep carbonate matrix. (*B*) Correlated SEM of the same microbial consortia shown in (*A*). (*C* and *D*) EDS analysis of the same consortia as in (*A*) and (*B*) showing carbon rich biomass (yellow, *C*) surrounded by Si-rich rings in blue (white arrows, *D*). Numbered points correspond to EDS point spectra (Dataset S1) taken to compare elemental composition of rings to amorphous silica spheres attached to ANME-SRB consortia shown in Fig. 3*A*.

similar to observations of Si on the surfaces of cyanobacterial cells (54). The silicification at cell surfaces is thought to be mediated by EPS and magnesium in cyanobacteria (55), and during the reductive dissolution of Fe^{3+}-rich clay minerals by metal-reducing *Shewanella oneidensis* (25, 57), which appear to share common textural characteristics with the amorphous silica phase reported here (25). Notably, the involvement of AMME-2/SRB consortia in extracellular electron transfer (EET) between partners (58) and, in some circumstances with iron or manganese oxides (e.g., ref. 59), may point to the local generation of conditions favorable for silicification facilitated by EET. Silicate precipitation concomitant with microbial respiration of Fe in clay minerals (57, 60) has been proposed to occur through interactions with polyamines (60). Long-chain polyamines (>7 aminopropyl units) can precipitate silica from silica oligomers in undersaturated conditions (61), which is mediated by bacteria under natural (62) and experimental (60) saturated silica conditions. Microbially mediated silicate precipitation has also been observed in the spore coat of *Bacillus subtilis*, in this case mediated by a serine- and arginine-rich protein (63). The zwitterionic nature of this protein conferred by serine and arginine residues is similar to that of silacidins and silaffins, proteins that mediate silica precipitation in diatoms (64, 65).

To explore potential biochemical mechanisms of Si-enriched mineral precipitation by ANME-SRB consortia, we screened the genomes (MAGs) of diverse ANME and syntrophic SRB assembled from metagenomic datasets (14, 66, 67). Following the approach of previous work targeting silaffin-like proteins in diatom genomes (68), we performed a search of our genomic database to find candidate proteins from ANME and SRB MAGs in sediment-free cultures with serine- and arginine-rich domains. We also searched our genomic database for homologs of aminopropyl transferases. However, no definitive homologs known to be associated with silicate precipitation were identified. The fact that there are currently several independent pathways for microbially mediated silica precipitation described suggests there are likely additional discoveries of biological mechanisms underlying this process. Different polyamines, such as copolypeptides with high block ratio of lysine and phenylalanine, polyallylamine, polyethylenimine, poly[acrylamide-co-2-(dimethylamino)]ethyl methacrylate or amine terminated dendrimers can act as templates for silica formation in vitro (69). Additionally, several posttranslational modifications (PTMs) have shown to be essential for the Si-precipitating property of silaffins, such as di- or trimethylation or alkylation of lysine residues with N-methylated oligo-propyleneimine chains, hydroxylation and phosphorylation of all the trimethylated lysine residues at the δ-position, and phosphorylation of all serine hydroxyl groups. The PTMs introduce a significant amount of both positive and negative charges, which render the peptide zwitterionic, a property critical for silica precipitation (70). These characteristics could be used as targets for searching and identifying potential proteins involved in this process. While the genomic mechanism currently remains elusive, our geochemical measurements (Fig. 3*B*) and modeling results (Fig. 3*C*) support the biologically mediated formation of Si-rich precipitates by AOM consortia in undersaturated conditions that is inconsistent with abiotic precipitation. Silicification relies on reactive cell surface ligands that can adsorb silica from solution, implying that cell surface charge may be critical for the initial silicification process (13). A neutral membrane, such as the one that enhances silica biomineralization in the cyanobacterium *Calothrix*, would be hydrophobic, thus enhancing the attachment of silica (38). For negatively charged cells, metal cation bridges (e.g., Fe^{3+}, Al^{3+}) might be necessary for silicification since the organic ligands at cell surfaces would be electrostatically repulsed to the negatively charged silica species (13). Notably, the potential for proton buffering by polymerized silica previously demonstrated in diatoms (71) may also benefit the ANME-SRB methanotrophic syntrophy, where proton build-up is predicted to occur during direct interspecies electron transfer, as electron transfer is faster than proton diffusion, resulting in local pH gradients (72, 73). We suggest that future research focuses on investigating cell or consortia surface charges (74), and differences in the functional groups between the cell wall and EPS, to gain further insights into the silica precipitation mechanisms used specifically by methanotrophic ANME-SRB consortia.

The mode of ANME-SRB biologically mediated silica precipitation of clay-related Si-rich phases described in this study may be important for the preservation of organic carbon in seep carbonates. Early diagenetic silica is observed in fossil seep carbonates spanning the Phanerozoic, where silica appears as fibrous and botryoidal cements replacing aragonite (49, 75–79). Early silica precipitation in seep carbonates can entomb organics; in one striking example, preservation of Cretaceous chemosynthetic symbiotic tube worm chitin in early silica cements has been documented (80). The observations that ANME-SRB consortia precipitate Si-rich phases both in laboratory enrichment cultures and what appears to be in situ within seep sediments and authigenic carbonates suggest that early amorphous silica cementation in seep carbonates may also improve the preservation potential of body

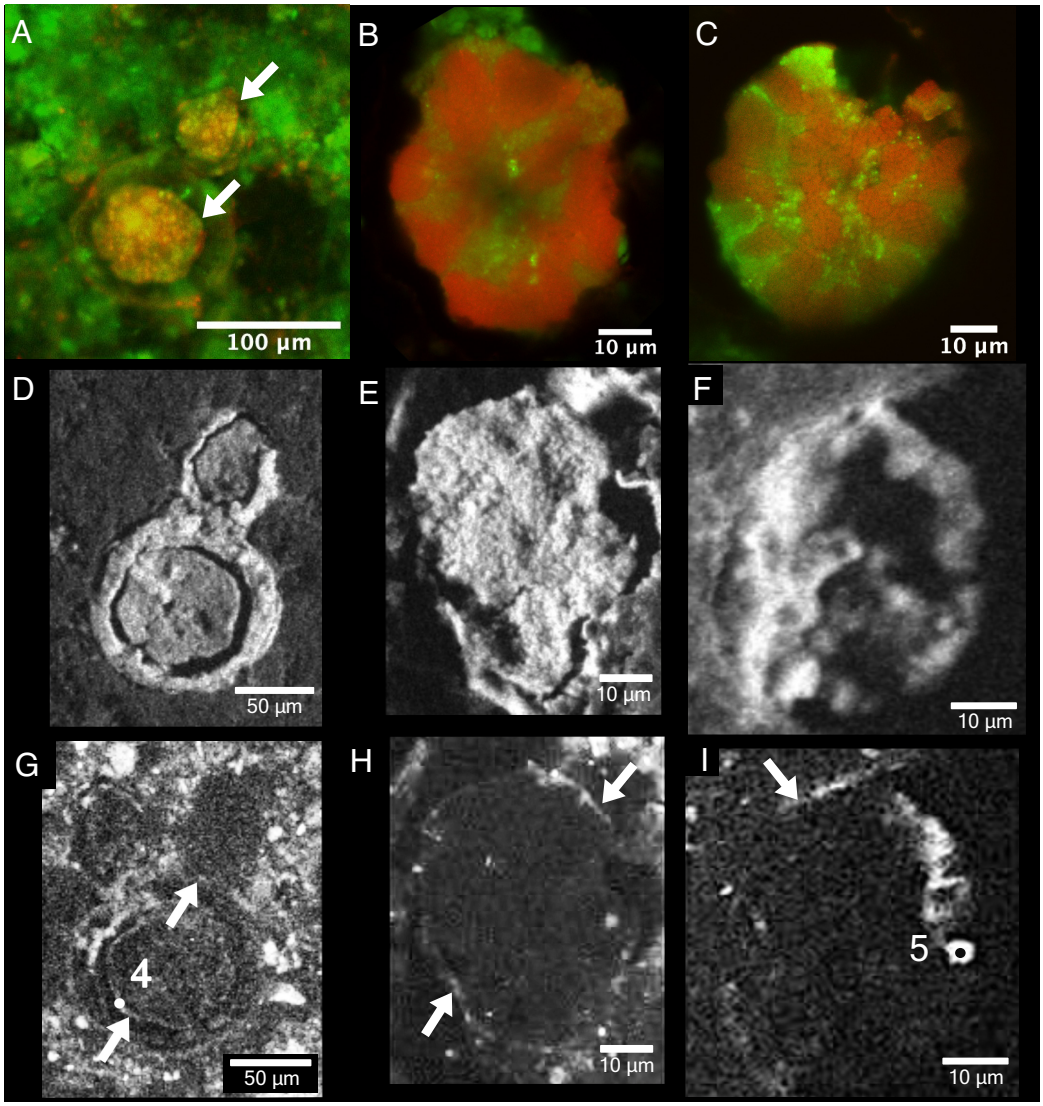

Fig. 5. Correlated epifluorescence microscopy and elemental analysis of ANME-2-SRB consortia and associated Si-rich phases in seep carbonate. (*A, B*, and *C*) FISH-stained endolithic ANME-2-SRB consortia (white arrows) embedded within the seep carbonate matrix. Cells hybridized with the ANME-2 [ANME-2-712 (52)] and SRB [DSS658 (1)] specific FISH probes are stained in red and green, respectively. (*D, E*, and *F*) Carbon maps from EDS analysis of the consortia shown in (*A, B*, and *C*), respectively. (*G, H*, and *I*) Silica maps from EDS analysis of the consortia shown in (*A, B*, and *C*), respectively. White arrows point at Si-rims surrounding the consortia. Numbered points correspond to EDS point spectra (Dataset S1) taken to compare elemental composition of rings to amorphous silica spheres attached to ANME-SRB consortia shown in Fig. 3*A*.

fossils and associated organics from ANME-SRB consortia in ancient seeps. We propose that future work could use Si-rich rings around carbonaceous domains in fossil seep carbonates as a search image to examine the potential preservation of ANME-SRB consortia preserved in the rock record.

Conclusions

Silicates have been found in association with ANME-SRB consortia, but a proof of their direct involvement in silicate biomineralization was lacking. We provide evidence for common occurrence of Si-rich phases in carbonate and sediment-hosted consortia and show precipitation of Si-rich phases with clay-like chemistry and morphology by actively growing ANME-2/SRB consortia in long-term AOM enrichment cultures. Our results suggest a direct role for methanotrophic microbial assemblages in the precipitation and evolution of silicate-bearing mineral structures, a process possibly distinct from observed microbially mediated silicate biomineralization in diverse microorganisms, all of which have poorly understood mechanisms. As the early precipitation of authigenic silicates is generally thought to improve the preservation potential of fossils (22, 81, 82), our results further support the possibility that massive chert precipitation as observed in classic microfossil localities such as the Gunflint (83) may not be critical for preserving microbial fossils in the rock record. Instead, microscale associations between microorganisms and amorphous Si-rich phases may provide adequate preservation potential, offering a search image in paleo-seep carbonates, and further serve as a geochemical trace fossil in the rock record.

Materials and Methods

Sample Collection and Processing. Sediment samples analyzed in this study were collected by push coring using the submersible HOV *Alvin* and, the R/V *Atlantis*, and the ROV *Doc Ricketts* of the R/V *Western Flyer* from three seafloor methane seep sites, including the Eel River Basin in Northern California (AT 15-11, October 2006), off the coast of Costa Rica (AT 37-13, May 2017), and in the Santa Monica Basin (October 2013). Push core (PC) samples PC14 and PC15 from

Alvin dive AD4254 (AT 15-11) were collected from a microbial mat proximal to an active methane seep site 520 m below sea level (mbsl) on the Northern Ridge of Eel River Basin (40.786533, −124.5951). Samples from the Costa Rica Margin (AT 37-13) were obtained during *Alvin* dive AD4912 from a microbial mat (PC 6) collected at 1,811 mbsl in the Jaco Scar submarine landslide (9.1163, −84.8372). Sediment samples (PC 43) from the Santa Monica Basin originated from a sulfide-oxidizing microbial mat covered seep site (33.788835, −118.668298) at 863 mbsl during dive DR 459. Samples were processed shipboard by extruding sediment from the push core liner and sectioning sediment at 3 cm intervals and either frozen at −80 °C, PFA-fixed for microscopy, or heat sealed under anoxic conditions in Ar-sparged mylar bags at 4 °C for laboratory-based microcosm experiments. Additionally, authigenic carbonate samples were collected from the Jaco Scar site using the submersible HOV Alvin and the R/V Atlantis (AT42-03, October–November 2018) for analysis of endolithic AOM consortia.

Density-based Separation of AOM Consortia from Sediments and Carbonates. Using a modified protocol (84), separation of ANME-SRB consortia from bulk sediment for downstream microscopy or cultivation was performed using a Percoll (Sigma-P1644) density gradient on an aliquot of seep sediment. Briefly, cells were disaggregated from bulk sediment by sonication for 3 × 10-s intervals on ice using a Branson Sonifier 50 with a power output of 4 W. The 1 mL aliquot of sonicated sediment was then pipetted onto 500 μL of a 100% Percoll density gradient and centrifuged at 18,000×*g* for 30 min at 10 °C using a Beckman–Coulter Microfuge 18 centrifuge. The supernatant (~1 mL) was then pipetted into 250 mL 1X PBS in a filter tower and vacuumed through a 5 μm polyethersulfone (PES) filter until ~50 mL solution remained in the tower, which was then diluted by ~200 mL 1X PBS added to the tower. Repeated filtration and dilution by 1X PBS was performed three times. We calculated this dilution and filtration to remove 99.2% of the 500 μL Percoll [initially containing 0.43 μmol Si (G.E. Healthcare Life Sciences, 2018)] present in the density separation supernatant, with the final filtration step yielding a 1-mL aliquot used for downstream microscopy. According to this calculation, final [Si] from Percoll should not exceed 3.4 μM. For microscopy, cells were initially fixed by incubating a 1 mL aliquot of sediment with 4% glutaraldehyde overnight at 4 °C. For cultivation, the procedures were done in an anaerobic chamber (Coy Laboratory Inc.) as previously described (14).

Establishment of a Sediment-free AOM Enrichment Culture and Seep Carbonate Incubations. The sediment-free enrichments of methane-oxidizing ANME-2 and SRB are described in Yu et al. (14) Briefly, the enrichments were maintained with a CH_4 headspace (2 bar) in 0.2 μm-filtered sterile defined artificial seawater media, which was exchanged periodically to remove metabolic by-products (i.e., bicarbonate, sulfide), while maintaining pH and replenishing sulfate.ANME-SRB consortia were separated from seep sediments by first homogenizing deep sea methane seep sediments (from Santa Monica Basin) with 0.2-μm filter-sterilized and Ar-sparged seawater collected above the sampling site, and transferred into N_2-sparged Pyrex bottles sealed with large butyl rubber stoppers as previously described (14). Percoll density separation under anoxic conditions was used to concentrate ANME-SRB consortia away from the sediment matrix, followed by anoxic filtration and washing on a 0.2 μm polycarbonate filter before transfer into N_2-sparged artificial seawater in butyl stoppered 125 mL serum bottles (sediment-free incubation; media composition from ref. 85). Field-collected deep-sea carbonate samples from Jaco Scar (Costa Rica margin) were placed in Pyrex bottles containing 0.2 μm filter sterilized N_2-sparged seawater from the site. Both carbonate microcosms and sediment-free AOM enrichments were supplied with a CH_4 headspace pressurized to ~2 atm and bottles were maintained in the dark at 10 °C. A partial exchange of spent media with the addition of 0.2 μm filter-sterilized Ar-sparged artificial seawater and CH_4 was conducted every 3 mo to remove sulfide. Sediment-free incubations were maintained in these conditions over ~5 y. Sulfate-reducing activity was monitored during the course of the incubations using a modified colorimetric Cline assay for hydrogen sulfide (86).

Fluorescence In Situ Hybridization (FISH) and Epifluorescence Microscopy of ANME-SRB Consortia Recovered from Methane Seep Sediments. Conventional fluorescence in situ hybridization (FISH) with a single fluorophore on the 5′ end was used to identify ANME-SRB consortia for analysis of consortium exteriors. In this study, cells fixed by glutaraldehyde and Percoll-separated were filtered down or dried onto 0.2 μm EMD Millipore white polycarbonate filters (Code GTTP) and incubated in 50 μL hybridization buffer for 24 h at the appropriate formamide stringency, following published protocols (87). Percoll separation was only performed on samples from sediment-bearing incubations. In this study, we used probes targeting general Archaea [Arch915 (88), ANME-2 [Eel932 (1), ANME--2a/b (89), and SRB [DSS658 (1). 4′,6-diamino-2-phenylindole (DAPI) was subsequently applied as a counterstain, and filters were illuminated using an XCite Series 120Q fluorescence source and imaged with a Qimage QIClick camera attached to an Olympus BX51 epifluorescence microscope using 60x (Olympus PlanApo N Oil, N.A. 1.42) and 100x (Olympus UPlan FL N Oil, N.A. 1.30) objectives. cellSens Dimension imaging software was used to acquire images. Epifluorescence image compositing was performed using the image processing software Q-Capture Pro 7.

NanoSIMS Analysis of ANME-SRB Consortia from Methane Seep Sediments. Sample preparation for NanoSIMS, analytical conditions, and image analysis were performed as described in McGlynn et al. (90). Briefly, AOM consortia from incubation # 3730 incubation were fixed with glutaraldehyde and prepared for TEM thin sectioning using the embedding resin Durcupan (90). The samples were cut at 500-nm thickness and placed on an indium tin oxide (ITO) wafer and gold coated. NanoSIMS analyses used a cesium (Cs+) primary ion beam at ~1.3pA. Secondary ion images ($^{12}C^-$, $^{13}C^-$, $^{12}C^{14}N^-$, $^{12}C^{15}N^-$, and ^{28}Si) were acquired using a range of raster sizes (10 μm to 47 μm at 512 × 512). The primary beam settings were D1 = 3 and either ES = 2 or 3. Presputtering was performed at D1 = 0, ES = 2 until $^{12}C^-$ counts were greater than 150,000 ct/s.

Fluorescence In Situ Hybridization Imaging of Endolithic ANME-SRB Consortia within the Seep Carbonate Matrix. An authigenic carbonate sample from Jaco Scar (Costa Rica margin) was incubated for 1 y under the conditions described above for the sediment-free enrichment cultures. A fragment of this carbonate was then fixed in 1% PFA overnight at 4 °C, washed with 1X PBS buffer, and embedded in Epoxicure 2 (Buehler Ltd.). The resin-embedded section was subsequently glued to a 1-inch round wafer, sectioned by rock saw, and polished with alumina polishing film of grits 60, 30, 12, 5, and 2 mm to achieve a rock section thickness of about 50 mm. For FISH, a dehydration series (50%, 75%, and 100% ethanol, 1 min each) was performed on the thin section, followed by hybridization with probes targeting ANME-2 [ANME-2-712 (52) and SRB [DSS658 (1) in 40% formamide hybridization buffer, as previously described (87). 5 μg/mL of a DAPI-Citifluor mounting medium was added prior to epifluorescence microscopy imaging. Epifluorescence pictures were taken with a fluorescence microscope (Elyra S.1, Zeiss) at 10x (EC Plan-Neofluar 10x/0.30 M27 objective) and 63x magnification (Plan-Apochromat 63x/1.4 Oil DIC M27 objective). Images were acquired using the Zen black software (Zeiss) and the image compositing was performed using the software Fiji (91).

Scanning Electron Microscopy of Putative AOM Consortia in Sediments and Carbonates. Scanning electron microscopy (SEM) and energy-dispersive spectroscopy (EDS) of ANME-SRB consortia immobilized on white polycarbonate filters were performed and correlated with optical microscopy. Additionally, sediment from each of the source sediments was filtered onto 0.2-μm EMD Millipore white polycarbonate filters (Code GTTP). These sediment samples and the rock thin section hybridized with DAPI/FISH were Pd-coated (10 nm thickness) using a Cressington Sputter Coater 208HR and examined using a Zeiss 1550VP Field Emission SEM equipped with an Oxford INCA Energy 300 X-ray EDS system. After SEM image acquisition, EDS mapping of AOM consortia was performed to characterize the spatial distribution of associated mineral phases. EDS point spectra were also collected to characterize the compositional range of consortium-adhered phases along with discrete particles from the sediment samples from which AOM consortia were extracted, allowing a comparison between consortium-attached silica phases and silicates not associated with consortia. SEM images were acquired using an electron beam energy of 10 eV and EDS mapping and spectra were acquired with an electron beam of 15 eV. Statistical analysis of EDS-acquired compositional data was performed in R.

TEM Analysis of AOM Consortia in Sediment-free Enrichment Cultures. ANME-SRB consortia from our sediment-free enrichments were embedded in hydrophilic resin following published protocols (90) and sectioned using a Leica Ultracut UCT ultramicrotome fitted with a diamond knife. Sections were stained using the contrasting agent osmium tetraoxide and subsequently imaged at the UC San Diego NCMIR facility using a FEI Spirit transmission electron microscope operated at 120 kV with a Tietz TemCam F224 2 K by 2 K CCD camera.

FIB-EDS. A cross-section of an ANME-SRB consortium recovered directly from seep sediment and identified by FISH was prepared using a focused Ga^+ ion beam (FEI Nova-600) at the Kavli Nanoscience Institute at Caltech, followed by EDS analysis of the FIB-sectioned consortium to acquire cross-sectional compositional variability of AOM consortium-attached silicates and consortium interiors.

ICP-MS. ICP-MS analysis was performed on an Agilent 8800 ICP-MS. ^{11}B, ^{27}Al, ^{43}Ca and ^{44}Ca were measured in no gas mode. ^{27}Al, ^{28}Si, ^{44}Ca, and ^{56}Fe were measured in oxygen gas mode via MSMS by detecting the oxide product at 16 m/z above the parent ion. Analyses of elements via different isotopes or analysis modes were consistent. Mixed elemental standards for ICP-MS were prepared by diluting 100 µL of the standard media to a final volume of 5 mL by a combination of elemental stock standards (Sigma-Aldrich) and 5% nitric acid in purified Type I water. Samples were prepared for ICP-MS analysis by diluting 100 µL of each sample to 5 mL using 5% nitric acid. This approach enabled determination of the measured elements via a standard addition analysis with accurate matrix matching. The slope of the response was then used to determine concentrations in the various incubated media samples.

Preparation of Mineral Stability Diagrams. We produced stability plots using the Geochemist Workbench software (Release 17) coupled with manual user guidance for mineral selection and equilibrium constants edits as needed. We included different mineral types that could be in equilibrium with log $\{Al^{3+}\}$ (−6.958) in the solution: clay minerals (beidellite, kaolinite, montmorillonite, and illite), feldspar minerals (albite and anorthite), chlorite minerals (chamosite and clinochlore), and quartz (amorphous and crystalline). The following are the log activities for the other ions used as constant values in the predominance diagram: log $\{Ca^{2+}\} = -3.488$, log $\{Mg^{2+}\} = -1.963$, log $\{Na^{+}\} = -0.475$, log $\{K^{+}\} = -2.204$, log $\{Fe^{+}\} = -6.699$, log $\{Mn^{2+}\} = -2.586$, and log $\{Cl^{-}\} = -0.408$. Consistent with the reported value for seawater, the calculated ionic strength was 0.68 M, considering all ions in the media. We considered that the pE of the solution of the solution was poised by the biological methane oxidation, leading to calculated pE values ranging from −3.64 at pH 6.5 to −6.14 at pH 9.0.

Data, Materials, and Software Availability. All data and custom scripts were collected and stored using Git version control. Code for raw data processing, analysis, and figure generation is available in the GitHub repository (https://github.com/daniosro/Si_biomineralization_ANME_SRB) (92). All other data are included in the manuscript and/or supporting information.

ACKNOWLEDGMENTS. We would like to acknowledge Jake Bailey, Tom Bristow, Ted Present, Paul Myrow, Kelsey Moore, and Jen Glass for contributing to discussions about this work and the thoughtful comments from K. Konhauser and anonymous reviewers who improved this work. We would like to thank Chi Ma for assistance with SEM-EDS, Yunbin Guan for assistance with NanoSIMS, and Nathan Dalleska for help with ICP-MS analysis. We are additionally grateful to Alice Michel for discussions regarding sample preparation for FISH-SEM. We further acknowledge the crews of R/V *Atlantis* and R/V *Western Flyer* for assistance in sample collection and processing. Funding for this work was provided by the US Department of Energy's Office of Science (DE-SC0020373), the NSF BIO-OCE grant (#1634002), a Gordon and Betty Moore Foundation Marine Microbiology Investigator grant (#3780), the Simons Collaboration for the Origin of Life, and a grant from the Center for Environmental Microbial Interactions (to V.J.O.). K.S.M. was supported in part by a NSF Graduate Research Fellowship and a Schlanger Ocean Drilling Fellowship. V.J.O. is a CIFAR science fellow in the Earth 4D program. Portions of this work were developed from the doctoral dissertation of Kyle Metcalfe, Symbiotic Diversity and Mineral-Associated Microbial Ecology in Marine Microbiomes; Anne Dekas, Diazotrophy in the Deep: An Analysis of the Distribution, Magnitude, Geochemical Controls, and Biological Mediators of Deep-Sea Benthic Nitrogen Fixation; and Daniela Osorio Rodriguez, Microbial Transformations of Sulfur: Environmental and (Paleo) Ecological Implications.

Author affiliations: [a]Division of Geological and Planetary Sciences, California Institute of Technology, Pasadena, CA 91125; [b]Earth-Life Science Institute, Tokyo Institute of Technology, Meguro, Tokyo 152-8550, Japan; [c]College of Urban and Environmental Sciences, Peking University, Beijing 100871, China; [d]Department of Earth System Science, Stanford University, Stanford, CA 94305; [e]National Center for Microscopy and Imaging Research, Center for Research in Biological Systems, University of California, San Diego, School of Medicine, La Jolla, CA 92093; and [f]Department of Civil and Environmental Engineering, McCormick School of Engineering and Applied Science, Northwestern University, Evanston, IL 60208

Author contributions: D.O.-R., K.S.M., J.P.G., and V.J.O. designed research; D.O.-R., K.S.M., S.E.M., H.Y., A.E.D., M.E., and T.D. performed research; D.O.-R., K.S.M., S.E.M., L.A., J.P.G., and V.J.O. analyzed data; and D.O.-R. and K.S.M. wrote the paper.

1. A. Boetius *et al.*, A marine microbial consortium apparently mediating anaerobic oxidation of methane. *Nature* **407**, 623 (2000).
2. V. J. Orphan *et al.*, Comparative analysis of methane-oxidizing archaea and sulfate-reducing bacteria in anoxic marine sediments. *Appl. Environ. Microbiol.* **67**, 1922–1934 (2001).
3. W. S. Reeburgh, Oceanic methane biogeochemistry. *Chem. Rev.* **107**, 486–513 (2007).
4. G. Wegener, R. Laso-Pérez, V. J. Orphan, A. Boetius, Anaerobic degradation of alkanes by marine archaea. *Annu. Rev. Microbiol.* **76**, 553–577 (2022).
5. R. Luff, K. Wallmann, Fluid flow, methane fluxes, carbonate precipitation and biogeochemical turnover in gas hydrate-bearing sediments at Hydrate Ridge, Cascadia Margin: Numerical modeling and mass balances. *Geochim. Cosmochim. Acta* **67**, 3403–3421 (2003).
6. S. J. Loyd *et al.*, Methane seep carbonates yield clumped isotope signatures out of equilibrium with formation temperatures. *Nat. Commun.* **7**, 12274 (2016).
7. N. Thiagarajan *et al.*, Stable and clumped isotope characterization of authigenic carbonates in methane cold seep environments. *Geochim. Cosmochim. Acta* **279**, 204–219 (2020).
8. J. J. Marlow *et al.*, Carbonate-hosted methanotrophy represents an unrecognized methane sink in the deep sea. *Nat. Commun.* **5**, 1–12 (2014).
9. O. U. Mason *et al.*, Comparison of archaeal and bacterial diversity in methane seep carbonate nodules and host sediments, eel river basin and hydrate ridge, USA. *Microb. Ecol.* **70**, 766–784 (2015).
10. Y. Chen *et al.*, Biomineralization mediated by anaerobic methane-consuming cell consortia. *Sci. Rep.* **4**, 1–9 (2014).
11. A. E. Dekas, *Diazotrophy in the Deep: An Snalysis of the Distribution, Magnitude, Geochemical Controls, and Biological Mediators of Deep-sea Benthic Nitrogen Fixation* (California Institute of Technology, 2013).
12. P. Michalopoulos, R. C. Aller, Early diagenesis of biogenic silica in the Amazon delta: Alteration, authigenic clay formation, and storage. *Geochim. Cosmochim. Acta* **68**, 1061–1085 (2004).
13. K. O. Konhauser, B. Jones, V. R. Phoenix, G. Ferris, R. W. Renaut, The microbial role in hot spring silicification. *AMBIO A, J. Hum. Environ.* **33**, 552–558 (2004).
14. H. Yu *et al.*, Community structure and microbial associations in sediment-free methanotrophic enrichment cultures from a marine methane seep. *Appl. Environ. Microbiol.* **88**, e02109-21 (2022).
15. K. S. Metcalfe, *Symbiotic Diversity and Mineral-Associated Microbial Ecology in Marine Microbiomes* (California Institute of Technology, 2021).
16. M. R. Walter, D. Desmarais, J. D. Farmer, N. W. Hinman, Lithofacies and biofacies of mid-Paleozoic thermal spring deposits in the Drummond Basin, Queensland, Australia. *Palaios* **11**, 497–518 (1996).
17. A. Channing, D. Edwards, Experimental taphonomy: Silicification of plants in Yellowstone hot-spring environments. *Earth Environ. Sci. Trans. R. Soc. Edinburgh* **94**, 503–521 (2003).
18. K. A. Campbell, Hydrocarbon seep and hydrothermal vent paleoenvironments and paleontology: Past developments and future research directions. *Palaeogeogr. Palaeoclimatol. Palaeoecol.* **232**, 362–407 (2006).
19. J. Peckmann, V. Thiel, Carbon cycling at ancient methane–seeps. *Chem. Geol.* **205**, 443–467 (2004).
20. J. J. Marlow *et al.*, Carbonate-hosted microbial communities are prolific and pervasive methane oxidizers at geologically diverse marine methane seep sites. *Proc. Natl. Acad. Sci. U.S.A.* **118**, e2006857118 (2021).
21. J. V. Bailey *et al.*, Pseudofossils in relict methane seep carbonates resemble endemic microbial consortia. *Palaeogeogr. Palaeoclimatol. Palaeoecol.* **285**, 131–142 (2010).
22. S. A. Newman, G. Mariotti, S. Pruss, T. Bosak, Insights into cyanobacterial fossilization in Ediacaran siliciclastic environments. *Geology* **44**, 579–582 (2016).
23. R. W. Renaut, B. Jones, J. J. Tiercelin, Rapid in situ silicification of microbes at Loburu hot springs, Lake Bogoria, Kenya rift valley. *Sedimentology* **45**, 1083–1103 (1998).
24. L. G. Benning, V. R. Phoenix, N. Yee, K. O. Konhauser, The dynamics of cyanobacterial silicification: An infrared micro-spectroscopic investigation. *Geochim. Cosmochim. Acta* **68**, 743–757 (2004).
25. G. Zhang, H. Dong, J. Kim, D. D. Eberl, Microbial reduction of structural Fe^{3+} in nontronite by a thermophilic bacterium and its role in promoting the smectite to illite reaction *Am. Mineral.* **92**, 1411–1419 (2007).
26. G. Sposito, *The Chemistry of Soils* (Oxford University Press, ed. 2, 2008).
27. K. O. Konhauser, M. M. Urrutia, Bacterial clay authigenesis: A common biogeochemical process. *Chem. Geol.* **161**, 399–413 (1999).
28. P. R. Girguis, A. E. Cozen, E. F. DeLong, Growth and population dynamics of anaerobic methane-oxidizing archaea and sulfate-reducing bacteria in a continuous-flow bioreactor. *Appl. Environ. Microbiol.* **71**, 3725–3733 (2005).
29. K. Nauhaus, M. Albrecht, M. Elvert, A. Boetius, F. Widdel, In vitro cell growth of marine archaeal-bacterial consortia during anaerobic oxidation of methane with sulfate. *Environ. Microbiol.* **9**, 187–196 (2007).
30. A. E. Dekas, R. S. Poretsky, V. J. Orphan, Deep-sea archaea fix and share nitrogen in methane-consuming microbial consortia. *Science* **326**, 422–426 (2009).
31. R. J. W. Meulepas *et al.*, Enrichment of anaerobic methanotrophs in sulfate-reducing membrane bioreactors. *Biotechnol. Bioeng.* **104**, 458–470 (2009).
32. V. J. Orphan, K. A. Turk, A. M. Green, C. H. House, Patterns of 15N assimilation and growth of methanotrophic ANME-2 archaea and sulfate-reducing bacteria within structured syntrophic consortia revealed by FISH-SIMS. *Environ. Microbiol.* **11**, 1777–1791 (2009).
33. I. Gunnarsson, S. Arnórsson, Amorphous silica solubility and the thermodynamic properties of H_4SiO_4 in the range of 0 to 350C at Psat. *Geochim. Cosmochim. Acta* **64**, 2295–2307 (2000).

34. R. Siever, N. Woodford, Sorption of silica by clay minerals. *Geochim. Cosmochim. Acta* **37**, 1851–1880 (1973).
35. K. O. Konhauser, W. S. Fyfe, F. G. Ferris, T. J. Beveridge, Metal sorption and mineral precipitation by bacteria in two Amazonian river systems: Rio Solimões and Rio Negro, Brazil. *Geology* **21**, 1103–1106 (1993).
36. K. O. Konhauser *et al.*, Mineral precipitation by epilithic biofilms in the speed river, Ontario, Canada. *Appl. Environ. Microbiol.* **60**, 549–553 (1994).
37. V. R. Phoenix, K. O. Konhauser, F. G. Ferris, Experimental study of iron and silica immobilization by bacteria in mixed Fe-Si systems: Implications for microbial silicification in hot springs. *Can. J. Earth Sci.* **40**, 1669–1678 (2003).
38. V. R. Phoenix, R. E. Martinez, K. O. Konhauser, F. G. Ferris, Characterization and implications of the cell surface reactivity of *Calothrix* sp. strain KC97. *Appl. Environ. Microbiol.* **68**, 4827–4834 (2002).
39. N. Yee, V. R. Phoenix, K. O. Konhauser, L. G. Benning, F. G. Ferris, The effect of cyanobacteria on silica precipitation at neutral pH: implications for bacterial silicification in geothermal hot springs. *Chem. Geol.* **199**, 83–90 (2003).
40. S. V. Lalonde, K. O. Konhauser, A.-L. Reysenbach, F. G. Ferris, The experimental silicification of Aquificales and their role in hot spring sinter formation. *Geobiology* **3**, 41–52 (2005).
41. R. C. Hugo, S. L. Cady, W. Smythe, The role of extracellular polymeric substances in the silicification of calothrix: Evidence from Microbial Mat Communities in Hot Springs at Yellowstone National Park, USA. *Geomicrobiol. J.* **28**, 667–675 (2011).
42. R. K. Iler, *The Chemistry of Silica: Solubility, Polymerization, Colloid and Surface Properties and Biochemistry of Silica* (John Wiley and Sons, 1979), 896p.
43. V. V. Annenkov *et al.*, Silicic acid condensation under the influence of water-soluble polymers: From biology to new materials. *RSC Adv.* **7**, 20995–21027 (2017).
44. S. E. McGlynn, Energy metabolism during anaerobic methane oxidation in ANME archaea. *Microbes Environ.* **32**, 5–13 (2017).
45. W. M. Berelson *et al.*, Anaerobic diagenesis of silica and carbon in continental margin sediments: Discrete zones of TCO_2 production. *Geochim. Cosmochim. Acta* **69**, 4611–4629 (2005).
46. E. Söding, K. Wallmann, *RV Meteor Cruise Report M54/2+3: Fluids and Subduction Costa Rica 2002; M54/2 Caldera - Caldera, August 13–September 7,2002, M54/3A Caldera–Caldera, September 10–September 28, 2002, M 54/3B Caldera–Curaçao, October 1–October 11, 2002; Investiga* (GEOMAR, 2003).
47. M. Lyle, I. Koizumi, M. L. Delaney, J. A. Barron, "32. Sedimentary record of the California current system, middle Miocene to Holocene: A synthesis of leg 167 results" in *Proceedings of the Ocean Drilling Program, Scientific Results*, M. Lyle, I. Koizumi, C. Richter, T. C. Moore, Eds. (2000), vol. **167**, pp. 341–376.
48. T. H. Naehr *et al.*, Authigenic carbonate formation at hydrocarbon seeps in continental margin sediments: A comparative study. *Deep Sea Res. Part II, Top. Stud. Oceanogr.* **54**, 1268–1291 (2007).
49. J. Peckmann, J. L. Goedert, V. Thiel, W. Michaelis, J. Reitner, A comprehensive approach to the study of methane-seep deposits from the Lincoln Creek Formation, western Washington State, USA. *Sedimentology* **49**, 855–873 (2002).
50. D. Osorio Rodriguez, *Microbial Transformations of Sulfur: Environmental and (Paleo) Ecological Implications* (California Institute of Technology, 2023).
51. V. J. Orphan, C. H. House, K.-U. Hinrichs, K. D. McKeegan, E. F. DeLong, Methane-consuming archaea revealed by directly coupled isotopic and phylogenetic analysis. *Science* **293**, 484–487 (2001).
52. K. Knittel, T. Lösekann, A. Boetius, R. Kort, R. Amann, Diversity and distribution of methanotrophic Archaea at cold seeps. *Appl. Environ. Microbiol.* **71**, 467–479 (2005).
53. D. M. Moore, R. C. Reynolds, *X-Ray Diffraction and the Identification and Analysis of Clay Minerals* (Oxford University Press (OUP), 1989).
54. K. R. Moore *et al.*, Biologically mediated silicification of marine cyanobacteria and implications for the Proterozoic fossil record. *Geology* **48**, 862–866 (2020).
55. K. R. Moore *et al.*, A new model for silicification of cyanobacteria in Proterozoic tidal flats. *Geobiology* **19**, 438–449 (2021).
56. V. Martin-Jézéquel, M. Hildebrand, M. A. Brzezinski, Silicon metabolism in diatoms: Implications for growth. *J. Phycol.* **36**, 821–840 (2000).
57. S. E. O'Reilly, J. Watkins, Y. Furukawa, Secondary mineral formation associated with respiration of nontronite, NAu-1 by iron reducing bacteria. *Geochem. Trans.* **6**, 1–10 (2005).
58. S. E. McGlynn, G. L. Chadwick, C. P. Kempes, V. J. Orphan, Single cell activity reveals direct electron transfer in methanotrophic consortia. *Nature* **526**, 531 (2015).
59. E. J. Beal, C. H. House, V. J. Orphan, Manganese- and iron-dependent marine methane oxidation. *Science* **325**, 184–187 (2009).
60. Y. Furukawa, S. E. O'Reilly, Rapid precipitation of amorphous silica in experimental systems with nontronite (NAu-1) and Shewanella oneidensis MR-1. *Geochim. Cosmochim. Acta* **71**, 363–377 (2007).
61. S. V. Patwardhan, G. E. Tilburey, C. C. Perry, Interactions of amines with silicon species in undersaturated solutions leads to dissolution and/or precipitation of silica. *Langmuir* **27**, 15135–15145 (2011).
62. J. H. Saw *et al.*, Encapsulated in silica: Genome, proteome and physiology of the thermophilic bacterium *Anoxybacillus flavithermus* WK1. *Genome Biol.* **9**, 1–16 (2008).
63. K. Motomura *et al.*, The C-terminal zwitterionic sequence of CotB1 is essential for biosilicification of the *Bacillus cereus* spore coat. *J. Bacteriol.* **198**, 276–282 (2016).
64. N. Kroger, R. Deutzmann, M. Sumper, Silica-precipitating peptides from diatoms. The chemical structure of silaffin-A from *Cylindrotheca fusiformis*. *J. Biol. Chem.* **276**, 26066–26070 (2001).
65. S. Wenzl, R. Hett, P. Richthammer, M. Sumper, Silacidins: Highly acidic phosphopeptides from diatom shells assist in silica precipitation in vitro. *Angew. Chem. Int. Ed.* **47**, 1729–1732 (2008).
66. C. T. Skennerton *et al.*, Methane-fueled syntrophy through extracellular electron transfer: Uncovering the genomic traits conserved within diverse bacterial partners of anaerobic methanotrophic Archaea. *mBio* **8**, e00530-17 (2017).
67. G. L. Chadwick *et al.*, Comparative genomics reveals electron transfer and syntrophic mechanisms differentiating methanotrophic and methanogenic Archaea. *PLoS Biol.* **20**, e3001508 (2022).
68. A. Scheffel, N. Poulsen, S. Shian, N. Kröger, Nanopatterned protein microrings from a diatom that direct silica morphogenesis. *Proc. Natl. Acad. Sci. U.S.A.* **108**, 3175–3180 (2011).
69. G. Della Rosa *et al.*, Tailoring of silica-based nanoporous pod by spermidine multi-activity. *Sci. Rep.* **10**, 21142 (2020).
70. C. C. Lechner, C. F. W. Becker, Silaffins in silica biomineralization and biomimetic silica precipitation. *Mar. Drugs* **13**, 5297–5333 (2015).
71. A. J. Milligan, F. M. M. Morel, A proton buffering role for silica in diatoms. *Science* **297**, 1848–1850 (2002).
72. X. He *et al.*, Microbial interactions in the anaerobic oxidation of methane: Model simulations constrained by process rates and activity patterns. *Environ. Microbiol.* **21**, 631–647 (2019).
73. A. E. Franks *et al.*, Novel strategy for three-dimensional real-time imaging of microbial fuel cell communities: Monitoring the inhibitory effects of proton accumulation within the anode biofilm. *Energy Environ. Sci.* **2**, 113–119 (2009).
74. M. Nishino *et al.*, Measurement and visualization of cell membrane surface charge in fixed cultured cells related with cell morphology. *PLoS ONE* **15**, e0236373 (2020).
75. T. Himmler, A. Freiwald, H. Stollhofen, J. Peckmann, Late Carboniferous hydrocarbon-seep carbonates from the glaciomarine Dwyka Group, southern Namibia. *Palaeogeogr. Palaeoclimatol. Palaeoecol.* **257**, 185–197 (2008).
76. A. Kaim, R. G. Jenkins, A. Waren, Provannid and provannid-like gastropods from the Late Cretaceous cold seeps of Hokkaido (Japan) and the fossil record of the Provannidae (Gastropoda: Abyssochrysoidea). *Zool. J. Linn. Soc.* **154**, 421–436 (2008).
77. R. R. Kuechler *et al.*, Miocene methane-derived carbonates from southwestern Washington, USA and a model for silicification at seeps. *Lethaia* **45**, 259–273 (2012).
78. D. Smrzka *et al.*, Constraining silica diagenesis in methane-seep deposits. *Palaeogeogr. Palaeoclimatol. Palaeoecol.* **420**, 13–26 (2015).
79. Y. Miyajima *et al.*, A late Miocene methane-seep deposit bearing methane-trapping silica minerals at Joetsu, central Japan. *Palaeogeogr. Palaeoclimatol. Palaeoecol.* **455**, 1–15 (2016).
80. Y. Hikida, S. Suzuki, Y. Togo, A. Ijiri, An exceptionally well-preserved fossil seep community from the Cretaceous Yezo Group in the Nakagawa area, Hokkaido, northern Japan. *Paleontol. Res.* **7**, 329–342 (2003).
81. R. H. T. Callow, M. D. Brasier, Remarkable preservation of microbial mats in Neoproterozoic siliciclastic settings: Implications for Ediacaran taphonomic models. *Earth-Science Rev.* **96**, 207–219 (2009).
82. T. Sallstedt, M. Ivarsson, H. Drake, H. Skogby, Instant attraction: Clay authigenesis in fossil fungal biofilms. *Geosci.* **9**, 32–39 (2019).
83. E. S. Barghoorn, S. A. Tyler, Microorganisms from the Gunflint Chert. *Science* **147**, 563–575 (1965).
84. V. J. Orphan, C. H. House, K.-U. Hinrichs, K. D. McKeegan, E. F. DeLong, Multiple archaeal groups mediate methane oxidation in anoxic cold seep sediments. *Proc. Natl. Acad. Sci. U.S.A.* **99**, 7663–7668 (2002).
85. S. Scheller, H. Yu, G. L. Chadwick, S. E. McGlynn, Artificial electron acceptors decouple archaeal methane oxidation from sulfate reduction. *Science* **351**, 1754–1756 (2016).
86. J. D. Cline, Spectrophotometric determination of hydrogen sulfide in natural waters. *Limnol. Oceanogr.* **14**, 454–458 (1969).
87. J. Pernthaler, F.-O. Glöckner, W. Schönhuber, R. Amann, Fluorescence in situ hybridization (FISH) with rRNA-targeted oligonucleotide probes. *Methods Microbiol.* **30**, 207–226 (2001).
88. D. A. Stahl, R. Amann, "Development and application of nucleic acid probes in bacterial systematics" in *Nucleic Acid Techniques in Bacterial Systematics*, E. Stackebrandt, M. Goodfellow, Eds. (John Wiley & Sons Ltd., 1991), pp. 205–248.
89. T. Treude, K. Knittel, M. Blumenberg, R. Seifert, A. Boetius, Subsurface microbial methanotrophic mats in the Black Sea. *Appl. Environ. Microbiol.* **71**, 6375–6378 (2005).
90. S. E. McGlynn *et al.*, Subgroup characteristics of marine methane-oxidizing ANME-2 Archaea and their syntrophic partners as revealed by integrated multimodal analytical microscopy. *Appl. Environ. Microbiol.* **84**, e00399-18 (2018).
91. J. Schindelin *et al.*, Fiji: An open-source platform for biological-image analysis. *Nat. Methods* **9**, 676–682 (2012).
92. D. Osorio-Rodriguez, "daniosro," Si_biomineralization_ANME_SRB. GitHub. https://github.com/daniosro/Si_biomineralization_ANME_SRB. Deposited 19 June 2023.